

Making MoE based LLM inference resilient with TARRAGON

Songyu Zhang
UC, Riverside

Aaron Tam
UC, Riverside

Myungjin Lee
Cisco Research

Shixiong Qi
University of Kentucky

K. K. Ramakrishnan
UC, Riverside

Abstract

Mixture-of-Experts (MoE) models are increasingly used to serve LLMs at scale, but failures become common as deployment scale grows. Existing systems exhibit poor failure resilience: even a single worker failure triggers a coarse-grained, service-wide restart, discarding accumulated progress and halting the entire inference pipeline during recovery—an approach clearly ill-suited for latency-sensitive, LLM services.

We present TARRAGON, a resilient MoE inference framework that confines the failure’s impact to individual workers while allowing the rest of the pipeline to continue making forward progress. TARRAGON exploits the natural separation between the attention and expert computation in MoE-based transformers, treating attention workers (AWs) and expert workers (EWs) as distinct failure domains. TARRAGON introduces a reconfigurable datapath to mask failures by rerouting requests to healthy workers. On top of this datapath, TARRAGON implements a self-healing mechanism that relaxes the tightly synchronized execution of existing MoE frameworks. For stateful AWs, TARRAGON performs asynchronous, incremental KV cache checkpointing with per-request restoration, and for stateless EWs, it leverages residual GPU memory to deploy shadow experts. These together keep recovery cost and recomputation overhead extremely low. Our evaluation shows that, compared to state-of-the-art MegaScale-Infer, TARRAGON reduces failure-induced stalls by 160–213 \times (from \sim 64 s down to 0.3–0.4 s) while preserving performance when no failures occur.¹

1 Introduction

Large Language Models (LLMs) have become a foundation of modern AI-powered applications (*e.g.*, conversation agents and code assistants). However, as model sizes grow into hundreds of billions of parameters, serving them at low latency and at reasonable cost is increasingly challenging. The Mixture-of-Experts (MoE) architecture tackles this challenge

by partitioning each dense feedforward network (FFN) layer into many smaller “experts” and using a “gating network” to activate only a subset of experts for each input token. By avoiding full-model activation on every token, MoE enables LLMs to scale total parameter capacity and throughput without a proportional growth in per-token compute cost [14, 21, 34].

As MoE serving scales to hundreds of GPUs, however, failures become increasingly common. Measurements from large-scale GPU deployments show non-trivial failure rates: for example, [9] reports an average per-node uptime of 99.5%, corresponding to around seven minutes of downtime per GPU node per day. So, in a 40-node (320 GPU) deployment like DeepSeek’s [26], this translates to roughly an 18.1% probability (*i.e.*, $1 - 0.995^{40}$) of at least one node outage at any given time. Even worse, [35] finds that GPU-related faults alone account for 27.05% of total system errors, representing the single largest failure source.

Unfortunately, today’s MoE serving systems are extremely brittle under such failures. In many systems, a single worker’s failure triggers a *coarse-grained* recovery: the entire inference job is torn down and restarted [16, 37], discarding all “in-flight” state (*e.g.*, partially constructed KV caches). Here, a “worker” refers to a process running on a GPU in a node participating in distributed inference, each typically executing a full transformer stack in monolithic serving engines (*e.g.*, vLLM [23]). This strategy scales poorly, as restarting hundreds of workers incurs long stalls, violates latency SLOs, and wastes computation already completed. The root cause of this behavior lies in the tightly synchronized, monolithic execution model adopted by existing inference frameworks that rely on synchronous collective communications. Thus, a single worker failure can trigger full restart—an approach ill-suited to interactive LLM services, where even sub-second disruptions degrade user experience.

Alternative: Decoupled attention and expert computation. A key observation is that MoE inference inherently decomposes the forward pass into two distinct computational roles. *Attention* modules maintain a per-request key-value (KV) cache (initialized during the prefill phase) and append to it

¹We will open source soon on github.

over time as decoding generates new tokens; In contrast, *expert* modules implement FFN layers whose execution is stateless and depends only on incoming token embeddings and expert weights (this holds in both prefill and decoding phases). This structural asymmetry suggests a natural way to define finer-grained failure domains: attention-side computation is stateful and benefits from careful checkpointing, while expert-side computation is stateless and can be replayed or migrated.

Modern MoE serving systems increasingly decouple attention and expert computation across different workers, rather than running a full transformer stack on each worker. This improves scalability and GPU utilization, as seen in systems such as MegaScale-Infer’s Disaggregated Expert Parallelism (DEP) [45], DeepServe [16], and others with a similar decoupled architecture [36, 42]. We refer to this pattern as *decoupled attention-expert deployment*, with Attention Workers (AWs) hosting attention modules and Expert Workers (EWs) hosting experts. However, despite this structural decoupling, these systems still rely on *tightly synchronized* execution between AWs and EWs. While this synchronous, batched execution achieves high GPU efficiency, it also *globally exacerbates the impact of failures* by stalling the entire inference pipeline.

Our Approach: TARRAGON. Building on these observations, we present TARRAGON, a resilient MoE inference framework that achieves stall-free, fine-grained failure recovery with minimal performance overhead. Rather than treating the entire inference job as a single failure domain, TARRAGON fully exploits the decoupled attention-expert deployment paradigm and separates AWs and EWs into distinct failure domains. The core objective of TARRAGON is: *When a failure occurs, TARRAGON confines its impact to the corresponding domain instead of restarting the entire job, allowing the rest of the inference pipeline to keep making forward progress without disruption.*

At a high level, TARRAGON makes two complementary design choices to serve its core objective. First, TARRAGON realizes distinct failure domains through a reconfigurable datapath between AWs and EWs. This datapath is implemented by a Reconfigurable Forwarding Engine (REFE) that mediates all AW-EW communication with an Expert Routing Table (ERT) that dynamically binds each *expert identity* (*i.e.*, the logical expert selected by the gating network) to *expert location* (*i.e.*, the physical EW/GPU hosting that expert). In many existing systems, this binding is static—each logical expert is permanently tied to a specific EW. As a result, when that EW fails, the expert itself becomes unavailable, forcing a pipeline-wide restart. In contrast, TARRAGON eliminates fixed bindings: AWs issue requests only in terms of logical expert IDs; REFE consults the ERT to resolve where each expert currently resides and routes the requests accordingly.

Second, to achieve non-disruptive failover, TARRAGON introduces a self-healing mechanism combined with new worker provisioning in parallel. Both mechanisms critically rely on having a failure domain at the granularity of an in-

dividual worker. Upon an AW or EW failure, self-healing keeps the pipeline running by reacting locally within each domain: quickly moving affected requests off failed workers onto healthy ones, so that the inference pipeline does not pause waiting for global recovery. In parallel, the TARRAGON’s control plane provisions replacement AWs/EWs and integrates them into the ongoing inference pipeline, restoring lost capacity.

Furthermore, to minimize the cost of recovery, TARRAGON tailors its failure resilience strategy to the different roles of AWs and EWs across the prefill and decoding phases. Because EWs are stateless in both phases (as discussed above), EW failures can be handled purely via replay on healthy EWs, accelerated by “shadow experts” that occupy available GPU memory but consume no compute resources. This design simplifies recovery to just reusing GPU-resident expert weights, avoiding costly reloads from storage.

For AWs, however, the cost of failure is phase-dependent. During prefill, recovery requires recomputing the KV cache from the prompt, which incurs extra work but does not disrupt an ongoing interaction. During decoding, by contrast, rebuilding the KV cache by replaying the full token history would introduce prohibitive latency. As we show in §2.2, prefill failures are relatively cheap, while decoding-time failures dominate recovery cost and are therefore our main optimization focus. To avoid this decoding phase penalty, TARRAGON performs *asynchronous, incremental* KV cache checkpointing and per-request restoration. TARRAGON also exploits short idle gaps on the AW-EW datapath to avoid interfering with normal traffic. This enables TARRAGON to resume decoding from the latest emitted token after an AW failure while keeping checkpoint bandwidth and compute overhead modest.

Contributions. This paper makes the following contributions:

- We analyze why existing MoE inference systems are brittle under failures (§2.2), showing how synchronous dependencies between AWs and EWs cause a single worker failure to stall the entire inference pipeline.
- End-to-end, TARRAGON’s self-healing combined with new worker provisioning reduces failure-induced stalls from ~ 64 s in a MegaScale-like baseline to 0.4 s for AW failures and 0.3 s for EW failures (160–213 \times improvement; §7.2).
- Under no failures, TARRAGON closely matches MegaScale-Infer in throughput and token-level latency (within 2.8%; §7.3); under failures, it achieves the above stall reductions without sacrificing steady-state performance.
- The asynchronous, incremental KV cache checkpointing has negligible overhead (< 3%) in the AW-EW datapath. The per-request restoration is able to reduce AW recovery latency by up to 1800 \times , recovery traffic by up to 8 \times , and eliminates any GPU recomputation that would be needed if we were to rebuild the entire KV cache.

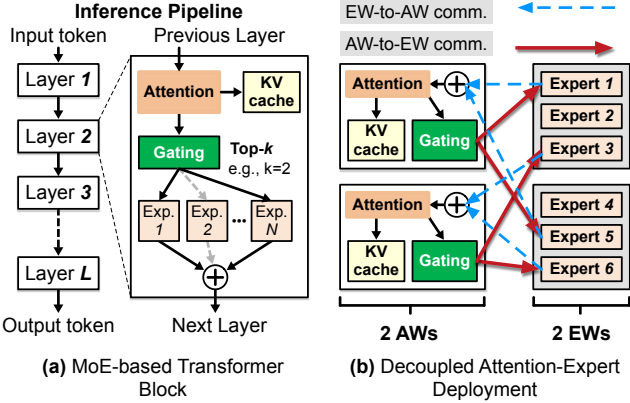


Figure 1: (a) MoE-based transformer layer and LLM inference pipeline: example shows top-2 experts selected; (b) decoupled attention-expert deployment.

2 Background and Motivation

2.1 Basics of MoE Inference

Transformers form the foundation of modern LLMs, comprising multiple self-attention and feed-forward network (FFN) layers stacked to improve compositional generalization and language modeling performance [31]. In conventional (dense) transformers, every token is processed by all FFNs in each transformer block. This dense activation causes both computation and memory costs to scale linearly with model size, making large models expensive to serve [14].

To address this limitation, recent LLMs adopt MoE-based models, which replace the dense FFN layer with a sparse MoE layer [4, 12, 30, 38, 39]. As shown in Fig. 1(a), an MoE layer consists of multiple FFNs (called *experts*) and a *gating network* that selects only the top- k experts for each token, typically with a small expert-selection ratio.² Each selected expert processes the token independently, and the resulting expert outputs are aggregated via a weighted sum using the gating weights before being passed to the next layer.

By activating a small subset of experts per token, MoE models increase total parameter capacity without proportionally increasing per-token compute cost, making them attractive for *inference* workloads [10, 24, 45]. In this work, we focus exclusively on MoE-based LLM *inference*; training-specific concerns are beyond the scope of this paper.

Prefill versus decoding. Inference naturally decomposes into two phases. During the *prefill* phase, the model consumes an input prompt (often hundreds or thousands of tokens) and builds the internal context state (KV cache). Prefill leverages substantial parallelism because tokens in the input sequence are all independent inputs [5]. During the *decoding* phase, the model generates output tokens sequentially, one token at a time. Each new token depends on all previously generated tokens, forcing decoding to proceed in a strictly sequential

²For instance, only 8 of 256 experts are activated in DeepSeek-v3 [26], and 8 of 128 in Qwen3-MoE [39].

manner at single-token granularity [5]. Despite their distinct execution characteristics, both phases traverse the same stack of transformer layers.

Stateful attention versus stateless expert. Transformers exhibit a fundamental asymmetry in how state is managed across attention and expert components. On the attention side, the model maintains a per-request KV cache that stores the key and value projections for all previously processed tokens. This cache is initialized during prefill and incrementally extended during decoding as new tokens are generated. As a result, attention computation is *stateful*: its execution depends on a growing context that persists across layers and across time.

In contrast, experts are stateless FFNs with fixed weights and no per-request persistent state. Given a batch of token embeddings, an expert’s output depends only on its input activations and its static parameters. This stateless property holds in both prefill and decoding: expert computation is a pure function that can always be reproduced by replaying the same inputs.

Deployment patterns for MoE inference. Early MoE serving systems often adopted a *monolithic* deployment model, where a single worker process (typically bound to one or more GPUs) hosts an entire transformer stack, including both attention and expert modules [23, 44]. Workers communicate via collectives (e.g., NCCL’s all-to-all [2]). While simple to implement, this design scales poorly in terms of memory efficiency and GPU utilization [45].

To address these issues, recent production systems [36, 45] have shifted to *decoupled attention-expert deployment*, in which attention and expert modules are placed on separate sets of workers (Fig. 1(b)). We refer to these as Attention Workers (AWs) and Expert Workers (EWs). This separation enables independent scaling of AWs and EWs, allowing expert traffic from many AWs to be consolidated onto fewer EWs to improve batching efficiency and GPU utilization.

In practice, AWs are typically scaled out using data parallelism [21, 36], with each AW serving a disjoint subset of requests, while EWs form an expert-parallel group that partitions expert FFNs across GPUs. Because AW-EW traffic follows an asymmetric many-to-many pattern rather than a

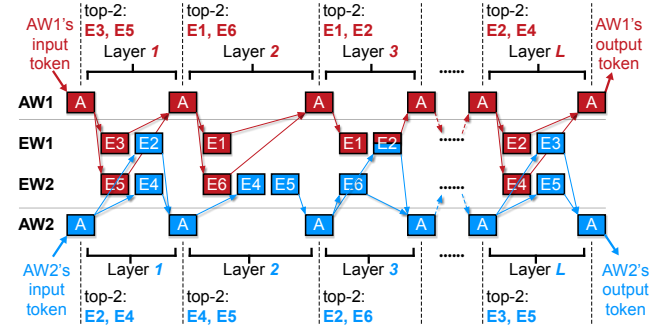


Figure 2: Example of layer-wise synchronized MoE inference. Here we show two data-parallel AWs, and two EWs, each hosting three expert FFNs (E1-E6), the same as Fig. 1(b).

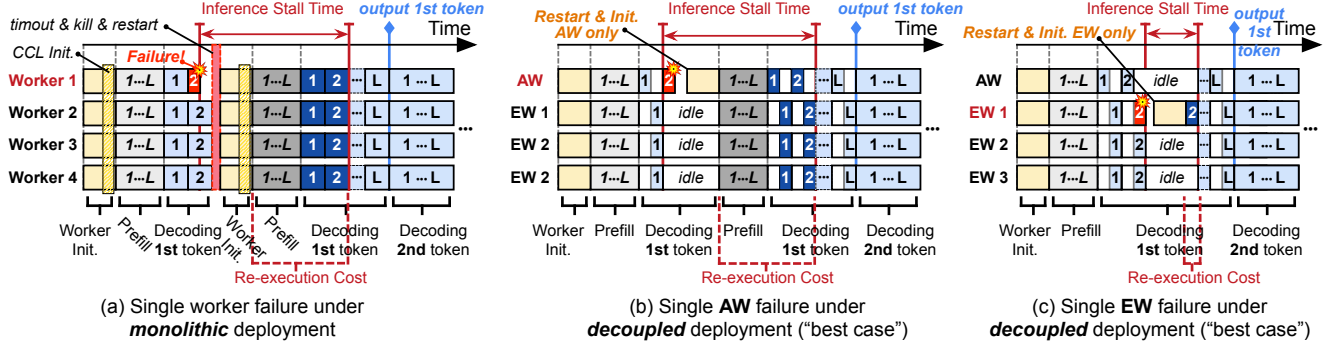


Figure 3: Coarse-grained failure recovery under different deployment modes. Numbers inside the “decoding” boxes denote the transformer layer currently being executed. For the decoupled deployment, we analyze a “best-case” recovery scenario, where a single worker failure restarts only the failed worker, thus effectively degrading to the monolithic case.

fixed symmetric collective, standard CCLs such as NCCL’s all-to-all are a poor fit [21, 36]. Recent systems therefore employ custom AW-EW data planes (e.g., MegaScale-Infer’s M2N) to support flexible expert routing and elastic scaling [21, 36].

2.2 Anatomy of Coarse-Grained Failures

To motivate the need for fine-grained, failure-resilient MoE inference, we first explain how layer-wise synchronization governs MoE execution, then analyze failure propagation under two representative deployment modes, and finally quantify the resulting recovery overheads.

2.2.1 Layer-wise synchronized execution

As described in §2.1, MoE inference advances layer by layer under a strict synchronization barrier between attention and expert computation. In decoupled deployments, this execution is distributed across AWs and EWs, as illustrated in Fig. 2.

Two important properties follow: (1) For each layer ℓ , every data-parallel AW independently processes its own request, selects a subset of experts, sends token embeddings to the corresponding EWs, and *waits until all selected experts return their outputs* (a synchronization barrier) before advancing to layer $\ell + 1$. We refer to the current layer index ℓ of an AW as its *frontier*; (2) On the EW side, GPUs execute expert FFNs in *layer-wise batches*: an EW aggregates requests for the same layer ℓ and expert, and executes them as a single large batch, and only then advances to the next layer. This layer-wise batching effectively ties EW progress to the same frontier as the AWs and is crucial for GPU efficiency [45]; naively executing each request immediately upon arrival destroys batching opportunities and severely underutilizes GPUs [45].

This layer-wise synchronization pattern holds across both prefill and decoding, and across both monolithic and decoupled deployments. Further, this layer-wise barrier is not tied to a particular parallelization scheme. Even under tensor or pipeline parallelism, each data-parallel AW group behaves as a logical “mega-AW” with the same layer-wise barrier.

2.2.2 Case studies and quantifying recovery overheads

We now examine how a single worker’s failure propagates under two representative MoE deployment modes discussed above.

We consider a failure during *decoding* an L -layer MoE model, while generating the i -th output token and executing layer ℓ ($1 \leq \ell \leq L$). This setting captures the worst impact on user-perceived latency, since the request has already gone through prefill and is in the middle of token generation.

Fig. 3(a)–(c) shows how a single worker failure escalates into a coarse-grained disruption.³ In all three cases, a single worker failure effectively induces a service-wide stall and the recovery incurs two fundamental penalties (highlighted in Fig. 3): (1) *Inference stall time* (T_{stall}), the duration during which the pipeline cannot generate new tokens for the affected request; (2) *Re-execution cost* (G), the amount of wasted GPU time/cycles required to recompute lost work. We now build a cost model to understand, *for a fixed model and deployment configuration*, how the *failure point* (captured by the decoded-token index i and the frontier layer ℓ) affects recovery cost. For clarity, we assume that workers are perfectly load-balanced and have comparable per-layer performance (thus, we ignore stragglers to keep the model simple).

Inference stall time. Let T_w be the average time to (re)initialize a worker, including process (or container) startup, CUDA context initialization, loading weights, and communication stack initialization [15, 28]. Let t_{pre} and t_{dec} be the average execution time of one prefill layer and one decoding layer for a single token, respectively. As shown in Fig. 3(a) and (b), the recovery procedure for a monolithic worker and for a decoupled AW has the same structure: the failed worker is restarted, then all workers must replay all prefill and decoding layers up to the failure point (i, ℓ) . In the monolithic deployment, a single worker failure also kills all healthy workers, as the collective communicator (CCL) treats the worker set as a static communication group and aborts when any

³We provide a detailed analysis of Fig. 3(a)–(c) in Appendix A.

worker is lost [46].⁴ Ignoring lower-order effects (e.g., warm caches, overlap), the stall time can thus be approximated as:

$$T_{\text{stall}}(\ell, i) \approx T_w + \underbrace{L \cdot t_{\text{pre}}}_{\substack{\text{Worker} \\ \text{Reinit.}}} + \underbrace{[(i-1)L + \ell] \cdot t_{\text{dec}}}_{\substack{\text{Replay } L \\ \text{prefill layers}}} \quad (1)$$

Replay decoding up to
layer ℓ of the i -th token

For a decoupled EW failure (Fig. 3(c)), prior prefill and decoding work is preserved on the AWs since EWs are stateless. Recovery only requires reinitializing the EW and re-executing the expert layer at the current frontier:

$$T_{\text{stall}}(\ell, i) \approx T_w + \underbrace{t_{\text{dec}}}_{\substack{\text{Worker} \\ \text{Reinit.}}} \quad (2)$$

Replay decoding
at frontier ℓ

Re-execution cost (GPU computation overhead). We measure GPU overhead in units of *GPU-time*, defined as the product of execution time and the number of GPUs (SMs) performing that recomputation. Let g_{pre} and g_{dec} denote the average per-worker GPU-time cost of processing one prefill layer and one decoding layer for a single token, respectively. For a monolithic deployment with M workers, all workers must replay the lost computation. Again, the decoupled AW failure follows the same replay pattern. The total GPU computation overhead is therefore:

$$G(\ell, i) \approx M \cdot \left[\underbrace{L \cdot g_{\text{pre}}}_{\substack{\text{Replay } L \\ \text{prefill layers}}} + \underbrace{((i-1)L + \ell) \cdot g_{\text{dec}}}_{\substack{\text{Replay decoding up to} \\ \text{layer } \ell \text{ of the } i\text{-th token}}} \right] \quad (3)$$

For a failed EW, only the expert computation at the current frontier must be repeated on a single replacement EW:

$$G(\ell, i) \approx g_{\text{dec}} \quad (4)$$

Experimental Setup for Audit. We validate this cost model using measurements from (1) a monolithic vLLM deployment and (2) a decoupled MegaScale-Infer-like deployment (configurations detailed in §7.1). Both systems serve the Mixtral-8×7B model (32 layers). The number of workers is 16 (8 AWs & 8 EWs for decoupled deployment). For each configuration, we empirically measure T_w , t_{pre} , t_{dec} , g_{pre} , and g_{dec} (see Table 1). We then sweep the failed decoded-token index i to evaluate recovery overhead across different decoding stages.

Fig. 4 shows the inference stall time and the re-execution cost, which reveals three observations: (1) For the failure of the monolithic worker and decoupled AW, stall time and wasted computation grow rapidly with the decoded-token index i : a failure later during decoding forces replay of a long history even when only one worker fails; (2) Decoding-time failures are the dominant concern: even when only 64 tokens

⁴In practice, this often manifests as a fatal NCCL/MPI error that terminates the job [46].

Table 1: Profiled parameters for the overhead analysis.

Deployment	T_w	t_{pre}	t_{dec}	g_{pre}	g_{dec}
vLLM [23]	24 s	1.68 ms	0.58 ms	0.010	0.0028
MegaScale-Infer [45]	18.5 s	2.18 ms	0.85 ms	0.006	0.0022

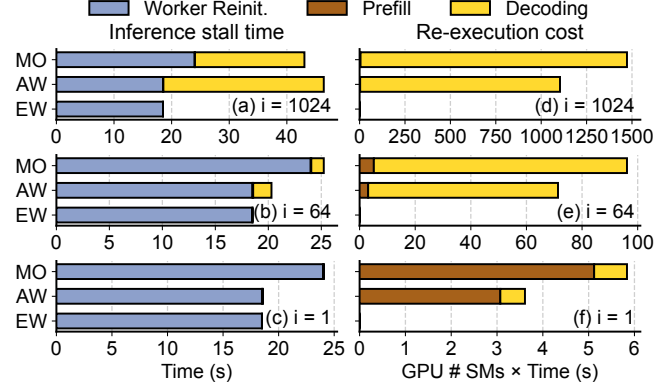


Figure 4: (a–c) Inference stall time and (d–f) re-execution cost under a single worker failure. MO: monolithic worker.

have been decoded, the recovery cost in decoding already exceeds that of a prefill failure with a 128-token prompt by about 19×, highlighting decoding as the primary target for optimization; (3) Although decoupled deployments limit the EW failure to single-layer re-execution, which introduces only a constant-time stall and the GPU overhead, the worker initialization cost T_w still remains on the critical path. Thus, EW failures can still introduce user-visible pauses even though the replay expense is small.

2.2.3 Takeaways

This analysis reveals three fundamental problems with the current failure handling in MoE inference:

- *Overly coarse failure domains.* Regardless of deployment modes, a single worker failure effectively enlarges the failure domain to the level of the full inference service, forcing all participating workers to restart or at least wait.
- *User-visible stalls.* Because the worker(s) must be restarted (T_w) and redo prefill and decoding before emitting new output tokens, recovery delays propagate directly to interactive users as broken conversational flows.
- *Wasted computation.* Previously computed KV cache and expert outputs are discarded and recomputed from scratch; the longer a request has been decoding when a failure occurs, the more GPU time is wasted.

Our goal in the rest of this paper is to design a MoE inference system that has **(D1) fine-grained worker-granularity failure domains**, **(D2) minimizes failure-induced stalls**, and **(D3) preserves as much useful computation as possible**.

3 Overview of TARRAGON

3.1 High-level Approach

TARRAGON achieves three major goals by rethinking how failures interact with the decoupled attention-expert deployment.

(D1): Reconfigurable worker-level failure domains. Although decoupled attention-expert deployments naturally suggest worker-granularity failure domains, existing systems fail

to realize this because placement and AW-EW routing are statically bound: each expert is pinned to a fixed GPU, and routing is baked into the datapath. TARRAGON breaks this static coupling and realizes **D1** with a *reconfigurable* AW-EW datapath (§4). Each AW dispatches requests through a Reconfigurable Forwarding Engine (REFE) that resolves logical expert IDs to physical EWs via an Expert Routing Table (ERT) (§4.2). Upon failure, the orchestrator updates the ERT to redirect traffic to healthy EWs without restarting AWs or pausing the pipeline. Meanwhile, EWs accept traffic from any AW without joining or recreating a collective group.

(D2): Self-healing and background capacity restoration. While reconfigurable routing prevents global restarts, it does not eliminate stalls ($T_{\text{stall}}(\ell, i)$ quantified in §2.2.2) caused by worker reinitialization and replay. To minimize such stalls, TARRAGON layers self-healing and background capacity restoration on top of its datapath. *Self-healing* decouples pipeline progress from worker recovery: when a worker (AW or EW) fails, its requests are immediately replayed on healthy alternatives rather than blocking until the failed worker reboots (§5.1, §5.2). For EWs, failover is further accelerated through shadow experts (§5.3), which are pre-loaded into residual GPU memory, so rerouting avoids costly reloads. In parallel, the orchestrator performs *background worker reprovisioning* (§5.4) to restore lost capacity without interrupting active inference. Together, these two mechanisms tackle the two dominant contributors to stall time identified in §2.2.2—worker restart delay T_w and long replay paths.

(D3): Efficient recovery for stateful AWs. Our cost analysis (§2.2.2) shows that *late* AW failures are especially expensive because KV caches must otherwise be rebuilt through replay (see Eq. (1) and (3)), adding stall time and GPU overhead. During this recovery, the attention module appends a small, fixed-size KV cache (denoted “segment” hereafter) for each token. TARRAGON mitigates this by introducing *asynchronous, incremental KV cache checkpointing* (§6.1) and *request-level KV cache restoration* (§6.2). AWs continuously stream newly appended KV cache segments to an external checkpoint store without interfering with the inference pipeline. Upon failure, the orchestrator only restores the affected requests’ KV caches on healthy AWs, shrinking recovery to “roughly one decoding layer at the current frontier” instead of replaying full prefill and decoding. This dramatically reduces both stall time (T_{stall}) and GPU recomputation (G).

3.2 TARRAGON Architecture

Fig. 5 summarizes TARRAGON’s architecture. Every AW has a Compute Engine (built atop vLLM) that hosts attention modules, manages the per-request KV cache, and interacts with EWs through the REFE, which implements the reconfigurable AW-EW datapath using the ERT. A single cluster gateway distributes user requests to the AWs. EWs host active and

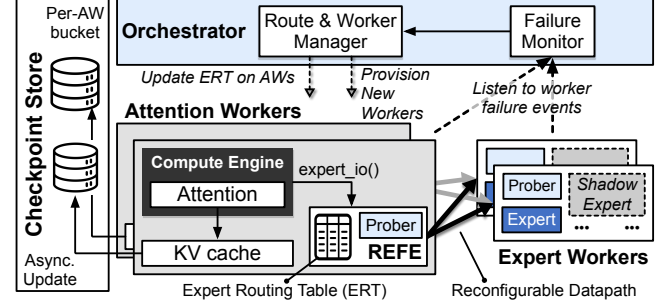


Figure 5: Overview of TARRAGON.

shadow experts. A centralized orchestrator monitors worker liveness for failure detection, includes a manager that updates the ERT on failures and joins, and coordinates background provisioning of new AWs and EWs. A checkpoint store receives incremental KV cache updates from AWs and serves request-level state to replacement AWs during recovery.

3.3 Failure Model

TARRAGON adopts a fail-stop failure model focused on hardware and software crashes. We assume workers (AWs and EWs) may fail due to application or OS crashes, node failures, power outages, and other unplanned interruptions. Of particular concern are CPU and GPU failures or errors requiring either a restart or a repair of the node. In practice, MoE serving clusters are GPU-heavy, so GPU device error is the dominant class of failures we target [9, 35]. TARRAGON also treats communication link failures as fail-stop events. Modern GPU clusters frequently experience link-level faults, *e.g.*, fabric-level connectivity loss and intra-node PCIe/NVLink disruption [7, 17, 35], which effectively isolate a worker even if its process is still running. In such cases, TARRAGON considers the affected worker unreachable and handles it similarly to a fail-stop crash. Byzantine failures are explicitly out of scope for this paper. Our detection and recovery mechanisms assume components are not malicious and that all the nodes (AW, EW, orchestrator) have a consistent (even if delayed) view of component failures.

4 Datapath for Fine-grained Failure Domains

The reconfigurable datapath in TARRAGON isolates failures at the worker level. As shown in Fig. 6, its key design aspects include the separation of control metadata from high-volume tensor transfers (§4.1), and the REFE that dynamically reroutes requests to healthy EWs upon failure detection (§4.2). TARRAGON currently implements its datapath using RDMA’s Reliable Connection (RC), which provides reliable delivery with hardware-assisted timeouts and retransmission.

4.1 Control and Data Planes

AWs and EWs in TARRAGON exchange both data (token embeddings) and small control messages required for fault

management. To avoid interference, TARRAGON allocates two Queue Pairs (QPs) per AW-EW pair: (1) a *control-plane QP* for liveness probes and self-healing metadata for rerouting and replay (§5.1–§5.2), and (2) a *data-plane QP* dedicated to bulk token embedding transfers. REFE uses the data-plane QP with GPUDirect RDMA to stream tensors directly into GPU memory, bypassing the CPU, for higher performance.

4.2 Reconfigurable Forwarding Engine

The Reconfigurable Forwarding Engine (REFE) is an AW-side runtime that coordinates point-to-point communication with EWs and orchestrates routing during inference. It exposes a simple API, *expert_io(expert_id, layer_id, token_embeddings)*, to abstract the underlying RDMA control and data planes. The compute engine invokes the API after completing its attention computation. Internally, REFE runs a non-blocking, event-driven execution loop that takes output tokens, consults the ERT, and dispatches metadata and token embeddings to the selected EWs.

Beyond request dispatching, REFE manages the reception of expert outputs from EWs and performs AW-side liveness probing. Missing or delayed EW responses are detected through these probes, triggering REFE’s self-healing logic (§5.1), which transparently replays requests to healthy EWs.

TARRAGON’s routing operates over point-to-point RDMA connections, giving each AW full flexibility to route individual requests to any EW without the reconfiguration of a collective communicator. This communication pattern resembles the M2N communication used in prior MoE systems [16, 27, 36, 45].

Expert Routing Table (ERT): TARRAGON decouples expert identity from expert location through the Expert Routing Table (ERT). The ERT maps each expert to one or more candidate EWs—potentially including shadow experts (§5.3)—allowing immediate rerouting when an EW fails or when additional EWs are provisioned with new expert replicas.

This indirection is the foundation of TARRAGON’s self-healing: routing adaptation becomes a localized remapping operation rather than a system-wide recovery. Each AW maintains its own ERT, updated by the orchestrator as the cluster evolves, ensuring that dynamic routing, fault isolation, and reconfiguration all occur with minimal disruption to ongoing inference.

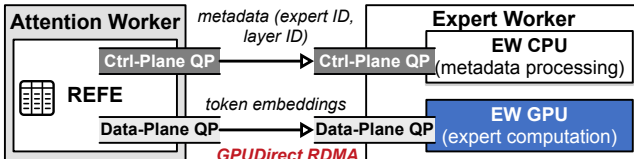


Figure 6: AW-EW datapath in TARRAGON. AWs dispatch requests to EWs through the REFE, which separates metadata and tensor transfers across two RDMA QPs.

5 Worker Failure Management

Lightweight Failure Detection. We build a hybrid liveness detection mechanism in TARRAGON: Tokens exchanged between AWs and EWs over their data-plane QPs serve as *implicit* heartbeat signals. If a data-plane connection remains silent for longer than a configured interval, the worker treats this as a potential indication of a failure and issues an *explicit* probe over the control-plane QP to confirm a peer’s liveness. This design avoids unnecessary probing under normal load but provides fast detection when failures occur (see additional implementation details in Appendix E).

5.1 How Does AW Tolerate EW Failures?

After an AW dispatches token embeddings to a selected EW, it waits for a response only for a bounded period. If the EW fails to respond within the timeout, REFE probes the loss of liveness and on detecting a failure, immediately reroutes the request to an alternate EW hosting the same expert (either a healthy primary or a shadow expert, §5.3).

Because expert computation is stateless and deterministic, replaying the same metadata and token embeddings produces identical results. This design allows REFE to mask EW failures immediately—without waiting for the orchestrator to trigger global recovery—while preserving uninterrupted inference execution. Replayed requests are prioritized at the destination EW to prevent recovering AWs from becoming stragglers. With this *AW-side self-healing*, EW failures no longer manifest as global synchronization barriers, as shown in Fig. 3(c): only AWs that were issuing requests to the failed EW perform local rerouting and replay, while other workers continue to make forward progress.

5.2 How Does EW Tolerate AW Failures?

In TARRAGON, EWs tolerate AW failures by starting expert computation once a *sufficient subset* of AWs has delivered their tokens, proceeding with partial inputs instead of waiting for all AWs to respond. Concretely, for each expert and layer, an EW buffers incoming tokens and starts the expert computation when either (i) it has received inputs from all AWs that are currently deemed healthy, or (ii) the buffered batch reaches a configured minimum size that preserves GPU efficiency.⁵ For any AW that has not contributed inputs within a short probing window, the EW issues liveness probes; if the AW is still unresponsive, it is treated as having failed for this layer, and its slots are simply omitted from the current batch. This *EW-side self-healing* design removes the implicit global barrier of prior MoE systems, where every EW must wait for inputs from *all* AWs before starting expert computation.

⁵Expert kernels reach near-optimal GPU efficiency at moderate batch sizes [45]. As we evaluated in Appendix B, once the expert batch exceeds a modest threshold, GPUs sustain high efficiency. Executing with slightly fewer tokens is thus an acceptable trade-off: it preserves GPU efficiency while avoiding the long tail latency induced by waiting for a failed AW.

5.3 Fast Expert Recovery via Shadow Experts

EW failures reduce the system’s expert capacity: when an EW crashes, all experts it hosts become unavailable until a replacement EW is provisioned and expert weights are reloaded, which can take hundreds of milliseconds to seconds [15].

TARRAGON introduces shadow experts that are pre-loaded but are normally *inactive* replicas of experts residing in EWs’ GPU memory. A shadow expert contains the same model weights and computation kernel as its primary, and can be activated immediately when the primary becomes unavailable. This allows TARRAGON to restore lost expert capacity almost instantaneously while the orchestrator provisions replacement EWs in parallel. We keep shadow experts inactive in the common case; keeping multiple experts active on the same GPU can cause kernel-level interference [1], increasing the expert’s execution latency (refer to Appendix D for additional analysis on the latency of having the shadow experts remain idle vs. executing in parallel).

GPU memory cost of shadow experts. Unlike AWs, EWs do not store the KV cache, so their footprint prior to activation is small. The main cost of shadow experts is GPU memory, which could be modest in practice. For example, a single DeepSeek-R1 expert occupies roughly 2.5 GB [11] for its weights, a relatively small proportion of the 40 to 80 GB capacity of GPUs such as an NVIDIA A100. Even with multiple active and shadow experts co-located, typical MoE configurations comfortably fit within device memory.

5.4 New Worker Provisioning

Introducing a new worker into the cluster includes: (i) connecting it to the existing AW-EW datapath, and (ii) synchronizing the new worker’s frontier (initialized at *layer 1*) with existing workers’ without interrupting their progress. A naive solution would let the orchestrator enforce a global frontier update, which is, however, hard to coordinate at sub-millisecond per-layer execution time (0.85 ms in Table 1).

Adding a new EW. When a new EW joins, the orchestrator updates all AWs’ ERTs. Each AW then sets up the datapath to the new EW. After connecting to all existing AWs, the new EW broadcasts a ready signal. From this point on, AWs may start routing tokens to the new EW whenever its

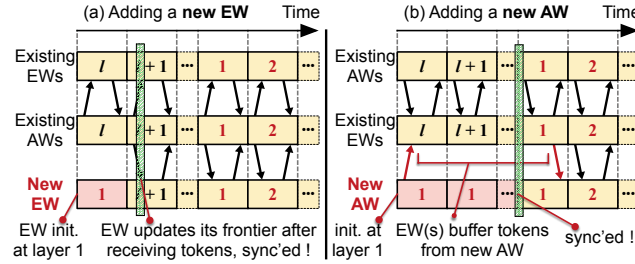


Figure 7: New (a) EW and (b) AW provisioning. Numbers inside the boxes denote the layer index.

experts are selected. Because existing AWs are already synchronized layer-wise, the first token the EW sees necessarily corresponds to the global frontier. As such, the EW updates its local frontier according to the layer index carried in the first token’s metadata (see Fig. 6), and then advances in lock-step with subsequent requests, as shown in Fig. 7(a).

Adding a new AW. The principle of adding a new AW is similar. The new AW boots and registers with the orchestrator to update its ERT. It then sets up the datapath to all EWs and it can immediately start serving *new* requests. However, when EWs first receive tokens from this AW, their own frontiers may be at some layer $\ell \neq 1$ for the current token. To preserve efficient layer-wise batching, EWs treat tokens from the new AW as follows: as shown in Fig. 7(b), they buffer these “early” tokens until they themselves wrap back to layer 1 for the corresponding experts, and then batch the buffered tokens together with layer-1 tokens from other AWs. From that point onward, the new AW is naturally synchronized at layer boundaries with the rest of the cluster.

This design (1) avoids global stalls: healthy workers never stop solely to accommodate a joining worker, unlike the coarse-grained recovery in Fig. 3; (2) preserves EW batching efficiency by letting both new EWs and new AWs join at layer-aligned points (next occurrence of layer 1).

6 KV Cache State Management

6.1 KV Cache Checkpointing

Initialization. When an AW starts, its compute engine allocates a contiguous KV cache region in GPU memory. REFE registers this region for RDMA, enabling one-sided remote writes into the checkpoint store. The AW then establishes an RDMA connection to the checkpoint store and sends the layout of its requested KV cache region (base address on the AW side and size). The checkpoint store allocates and registers a dedicated memory bucket for this AW and returns the base address on the checkpoint store side. Because both sides allocate fixed contiguous buffers, the AW can compute the remote write offset for the new KV cache, enabling direct one-sided updates without any receiver-side CPU involvement.

Asynchronous incremental updates. For every layer, the AW incrementally updates one KV segment for each token. When the KV cache segment is updated, the compute engine notifies REFE through a non-blocking `async_update()` call, passing the address range of the new segment. REFE then asynchronously issues a one-sided RDMA write that transfers this segment into the AW’s bucket in the checkpoint store.

One-sided RDMA writes make checkpointing scalable but do not guarantee that segments arrive in order at the checkpoint store; Later segments may arrive before earlier ones, making the checkpoint unusable for recovery. To enforce ordering, TARRAGON adopts a standard “async log + commit record” design, similar to RDMA-backed write-ahead log

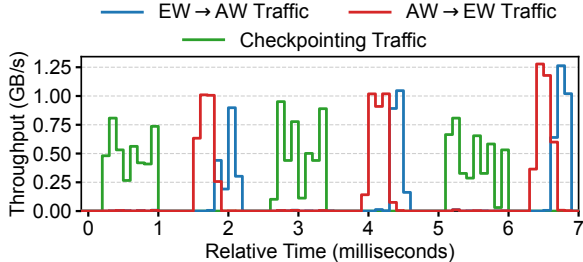


Figure 8: Traffic pattern with incremental checkpointing.

ging in prior systems [13, 22, 41]. Each update is tagged with a *sequence number* to preserve ordering, implemented as a monotonically increasing RDMA work request ID.

Opportunistic interleaving with AW-EW traffic. The checkpointing mechanism must run without interfering with the AW-EW traffic that drives the inference progress. In practice, we find that AW-EW communication is highly *bursty*, as shown in Fig. 8. This is measured using the Mixtral-8×7B model. Refer to §7.4 for testbed setup. Here we show a trace for a request arrival rate of 10 RPS, but we observe a similar pattern at other rates: the link is heavily used when AWs scatter/gather expert inputs and outputs, but remains largely idle while AWs execute attention computation for the same layer. These recurring idle intervals provide natural windows for incremental KV cache updates, that don’t contend with AW-EW traffic. TARRAGON schedules incremental KV cache checkpoints just within these gaps.

6.2 Request-Level KV Cache Restoration

TARRAGON recovers only the affected requests through the per-request KV cache restoration. Upon detecting an AW failure, the orchestrator identifies all active requests on the failed AW by noting the latest committed token stored in the checkpoint store. The orchestrator redistributes these requests to alternate AWs, typically in a round-robin manner to balance the load.

For each reassigned request, recovery proceeds as follows. The checkpoint store sends the alternate AW the request’s committed token ID and the size of KV state to restore. The AW allocates a fresh per-request region in its KV cache and returns the offset to the checkpoint store. Using GPUDirect-based one-sided RDMA writes, the checkpoint store then injects the KV cache segments directly into the AW’s GPU memory, followed by an HTTP request to confirm completion.

After the KV cache is reconstructed, the alternate AW resumes decoding from the committed token as if the request had been executed locally. Restoration is fully parallelized with the ongoing inference, because each request maintains its own isolated region. As a result, TARRAGON recovers AW failures without global rollback and without disrupting the progress of unrelated requests.

7 Evaluation

Our evaluation is based on measurements of our implementation of TARRAGON running in NSF CloudLab and Google Cloud.

Implementation. We implement TARRAGON (about 16K lines of C++ code and 2K lines of Python). For the AW, we use vLLM [23] as the compute engine for both prefill and decoding, with the REFE implemented as a C++ extension with a Python shim. EW is written from scratch in C++ using libtorch (PyTorch’s C++ API) for expert computation and libibverbs for RDMA. The orchestrator is a C++ control plane service exposing HTTP endpoints for configuration and failure monitoring of workers. The checkpoint store is implemented as a separate C++ service using libibverbs. We will open source soon.

We aim to answer the following questions:

- How much can TARRAGON reduce user-visible stalls under worker failures compared to coarse-grained restarts? (§7.2)
- What is the steady-state cost of adding failure resiliency, in terms of throughput and token-level latency, when no failures occur? (§7.3)
- How much overhead do TARRAGON’s individual resiliency components introduce by themselves? (§F)
- How effective and lightweight are TARRAGON’s KV cache checkpointing and restoration mechanisms? (§7.4)

We compare TARRAGON against two state-of-the-art MoE serving frameworks, (monolithic) vLLM [23] and (decoupled) MegaScale-Infer [45]. Both don’t have fine-grained resiliency and have to rely on coarse-grained restarts after failures.

7.1 Experimental Setup

Testbed: Unless otherwise noted, our experiments run on three Google Cloud (GCP) A3 Ultra nodes. Each node has 224 vCPUs, 3 TB RAM, eight H200 GPUs (141 GB memory), and eight 400 Gbps ConnectX-7 RDMA NICs with GPUDirect RDMA and intra-node NVLink (3.6 Tbps) enabled. All experiments run Ubuntu 22.04 with Linux 5.15, CUDA 12.8 (driver 580), and PyTorch 2.6.0.

Model and workloads. We evaluate TARRAGON on Mixtral-8×7B [20], a 32-layer MoE transformer with 8 experts per MoE layer and top-2 experts selected. We use two prompt-completion workloads: ShareGPT [3], with naturally varying input prompt lengths that examine both prefill and decode with realistic request heterogeneity; and a synthetic workload with randomly generated fixed-length prompts (10 input tokens, 128 generated tokens) to emphasize the decoding phase (called “Random”). Request arrivals follow a Poisson process with varying rates to emulate different load levels.

Configuration of Baselines: For MegaScale-Infer, we follow its decoupled design and place 8 AWs on one A3 Ultra node and 8 EWs on the other node, so that all AW-EW traffic traverses inter-node RDMA links. To match MegaScale-Infer’s setting, TARRAGON uses the same 16 GPUs (8 AWs + 8

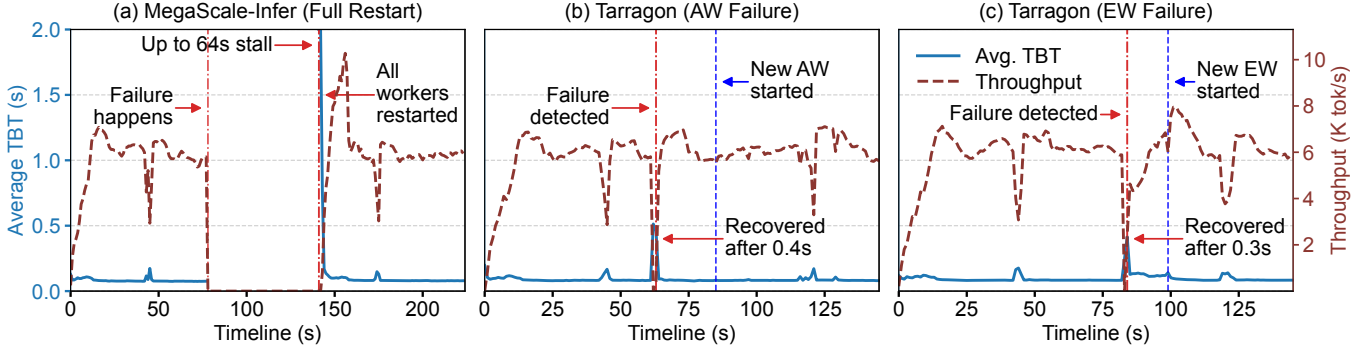


Figure 9: End-to-end failover behavior in terms of time-between-tokens (TBT) and output tokens per second under a single worker failure. Note that (a) uses a longer time range than (b) and (c) because the MegaScale-style baseline experiences a much longer stall; thus, we run it longer to ensure performance has fully recovered after failover.

EWs on the first two nodes) and an additional node only for the checkpoint store, so it does not benefit from extra GPU capacity. For monolithic vLLM, we adopt the two standard configurations that best exploit its design: vLLM-TP with tensor parallelism degree 16 and vLLM-PP with a 16-stage pipeline. Both vLLM baselines are deployed on two A3 Ultra nodes with a total of 16 GPUs, leveraging intra-node NVLink for fast GPU-GPU communication (the recommended practice for TP/PP-style multi-GPU inference). All systems share the same backend kernels and batching policy for a fair comparison, and disable any optimizations not common to all. TARRAGON does failure probing every 10 ms; the baselines do not have failure detection.

7.2 End-to-End Failover Behavior

Setup: We first focus on failover behavior in the decoding phase, during which the model emits tokens under tight latency constraints. We use the “Random” workload, which stresses the decoding phase, and set the request arrival rate to 50 RPS to keep the system under moderate load, so that observed stalls mainly reflect failover behavior rather than overload. We compare TARRAGON against MegaScale-Infer. Our primary metrics are the *time between tokens* (TBT) and inference throughput (output tokens per second). Increased TBT during failures will be perceived by users as the disruption in the stream of responses.

For each run, we start a long-running interactive request stream and let the pipeline reach the steady-state decoding phase. Around 60–80 s after the first request is issued, we inject a fail-stop worker failure by sending SIGINT to one worker process. For TARRAGON, we evaluate two failure scenarios separately: (i) failure of a single AW, and (ii) failure of a single EW. In both cases, TARRAGON’s self-healing mechanisms will provision a new worker in the background. **Results:** Fig. 9(a) shows the TBT and throughput timeline for the MegaScale-Infer. When the failure is injected at 78 s, the throughput immediately drops to zero. The system kills and restarts all workers, reloads model weights, and reruns both prefill and decoding before it can emit the next token. The

stall lasts for roughly 64 s, consistent with our cost model in §2.2.2, and is visible to the user as a frozen response stream.

Figs. 9(b) and (c) show the corresponding behavior under TARRAGON. When an AW fails, TARRAGON’s self-healing reroutes the affected request to healthy AWs and replays only the minimal state needed at the current frontier. The resulting stall (and period during which throughput drops) is only about 0.4 s, a 160× reduction compared to the baseline. When an EW fails, TARRAGON masks the failure by replaying expert computation to healthy EWs and shadow experts, while a replacement EW is provisioned in the background. While waiting for the replacement EW, the reduced capacity results in a slightly elevated TBT. But, the actual stall in the token stream is substantially reduced, to just about 0.3 s, or 213× shorter than the baseline. In both cases, token generation resumes more quickly compared to the minute-long pause. After the new EW’s initialization, it joins the cluster. The TBT returns to its pre-failure level. This behavior is precisely what TARRAGON is designed to achieve: *self-healing hides the long worker initialization latency from users, while background provisioning fairly quickly restores the original capacity*.

7.3 Is There a Cost to Failure Resiliency?

Setup: We now compare TARRAGON against three non-resilient baselines: vLLM-TP, vLLM-PP, and MegaScale-Infer, under non-failure conditions. We vary the load from 30 to 70 RPS and report (i) TTFT (time-to-first-token) and TBT (median and P95), (ii) output-token throughput for both ShareGPT and Random workloads.

TTFT (Fig. 10, top row). For prefill, TARRAGON closely tracks MegaScale across loads on both workloads, indicating that TARRAGON’s resiliency adds negligible startup latency. But, the two vLLM baselines show different behaviors. At low to moderate load (30–40 RPS), vLLM-TP achieves slightly lower TTFT than the decoupled systems. This is helped by its use of high-bandwidth NVLink for intra-node communication, so prefill completes quickly when the cluster is not saturated. However, as load increases beyond 40 RPS, vLLM-TP’s TTFT grows very sharply, reaching multi-second delays. vLLM-PP

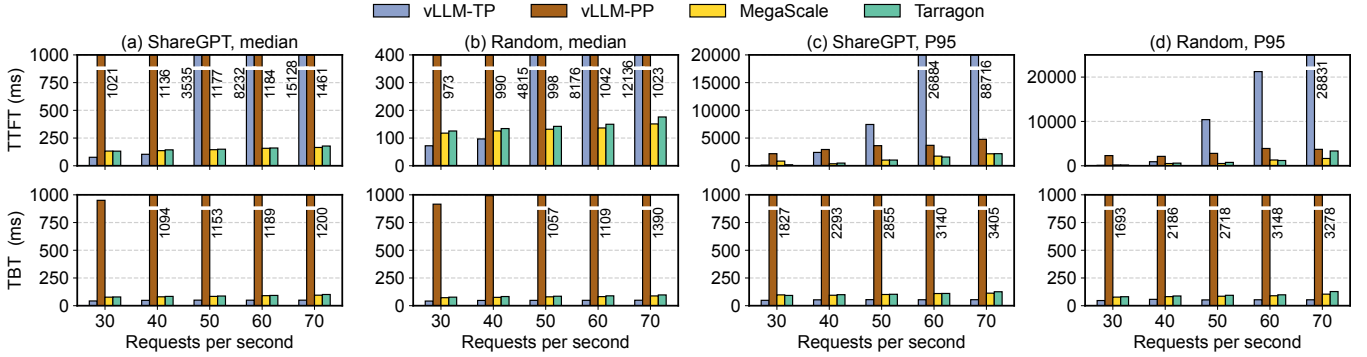


Figure 10: Cost of failure resiliency on token-level latency. Top: TTFT. Bottom: TBT. We report medians (a-b) and P95 (c-d) across ShareGPT and Random workloads as load increases (30-70 RPS).

exhibits consistently worse TTFT than both MegaScale and TARRAGON at all loads.

TBT (Fig. 10, bottom row). For decoding, TARRAGON and MegaScale again remain close. The differences among vLLM baselines are mainly driven by how well their parallelism strategies fit autoregressive decoding. vLLM-PP shows substantially larger TBT across all loads. vLLM-TP generally achieves slightly better TBT than the decoupled systems. By splitting each transformer layer across GPUs and using NVLink-backed collectives to gather partial results, vLLM-TP can keep its GPUs busy and hide much of the intra-node communication cost. In contrast, MegaScale and TARRAGON must perform AW-EW scatter/gather over inter-node RDMA links; this additional network hop introduces a small but visible latency penalty per token.

Output-Token Throughput (Fig. 11). TARRAGON essentially matches MegaScale’s throughput (with a deviation within 2.8%). vLLM-PP and vLLM-TP deliver consistently lower throughput: pipeline parallelism leaves some GPUs underutilized due to pipeline bubbles and imbalance, while tensor parallelism pays per-layer collective overhead across the GPUs, which limits the effective throughput at high load.

Takeaway. These results demonstrate that TARRAGON preserves the performance benefits of decoupled deployment, matching MegaScale-Infer in latency and throughput across various loads and workloads. It outperforms monolithic vLLM-TP/PP in most settings—while adding strong failure resiliency with little or no additional cost in the no-failure common case.

We also conduct an ablation study to quantify the steady-

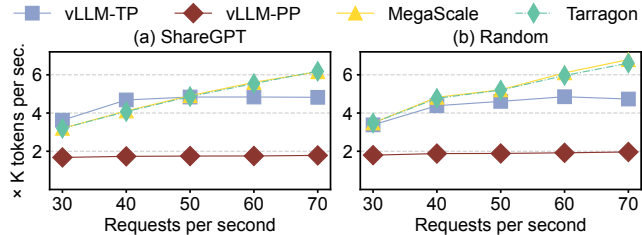


Figure 11: Cost of failure resiliency on output tokens per second (higher is better) for (a) ShareGPT and (b) Random.

state overhead of incremental KV cache checkpointing, lightweight failure detection, and ERT-based expert remapping, on TARRAGON’s end-to-end throughput without injecting failures. The results showed that across all request rates and workloads, the throughput of all alternatives are nearly indistinguishable: the maximum difference is less than 3% (details are in Appendix F).

7.4 KV cache Checkpointing and Restoration

We perform this experiment on three GCP A3 Ultra nodes (§7.1), where AWS, EWs, and checkpoint stores run on separate nodes with RDMA NICs interconnecting them.

Overhead of different checkpointing schemes. Our goal here is to understand whether different checkpointing schemes interfere with the inference, in particular whether TARRAGON’s can preserve inference throughput while providing fine-grained checkpointing. We consider two baselines: (1) *No checkpointing*, which serves as the upper-bound baseline; (2) *Pause-Checkpoint-Resume*, which periodically stalls inference to take a global snapshot of *all* KV cache pages (the training-style approach), and then resumes decoding.

For *Pause-Checkpoint-Resume*, we vary the checkpoint interval by the number of generated tokens: after every X decoded tokens, the system pauses, checkpoints the whole KV cache, and then resumes. TARRAGON does not use such periodic intervals. In TARRAGON, once a token’s KV segment has been updated, the AW immediately checkpoints it, during which AW-EW traffic is naturally idle (Fig. 8).

We report end-to-end inference throughput in output tokens per second. Without checkpointing, the system achieves 1148 tokens/s. With TARRAGON’s asynchronous incremental checkpointing, throughput is 1147 tokens/s, essentially identical to *no checkpointing*. This confirms that opportunistic interleaving is effective: KV cache updates occur during link idle periods and do not measurably interfere with normal AW-EW communication.

In contrast, *Pause-Checkpoint-Resume* incurs significant overhead even at relatively coarse intervals. With a checkpointing interval of once every 8 tokens, throughput drops by $2.15 \times$ compared to both *no checkpointing* and TARRAGON.

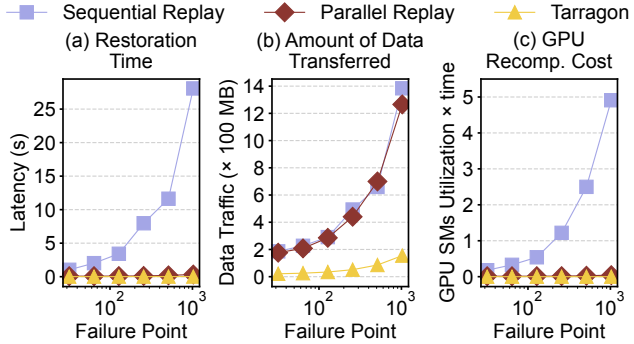


Figure 12: Impact of different restoration strategies at varying failure points.

The degradation stems from repeated global stalls: each checkpointing pauses the entire pipeline, blocking new token generation while KV-state is flushed. Achieving token-level checkpointing with *Pause-Checkpoint-Resume* would require even more frequent stalls and thus be prohibitive for interactive inference.

AW restoration. We evaluate how TARRAGON’s per-request KV restoration impacts AW-side self-healing during decoding-time failures. We focus on a single AW failure during the decoding phase (since it dominates user-perceived impact) and compare against two replay-based baselines: (1) *Sequential replay*: an alternate AW rebuilds the lost KV cache by rerunning prefill and then *sequentially* decodes all tokens from the beginning up to the failure point, without using any checkpoints. (2) *Parallel replay*: an alternate AW performs the prefill over the original prompt plus all tokens generated up to the failure point, reconstructing the lost KV cache in *parallel* rather than token by token.

We vary the *failure point*, which is defined as the index of the token being decoded when the failure occurs. A larger failure point corresponds to a larger number of decoded tokens and a larger KV cache to recover. For each strategy, we measure: (1) the total restoration time, (2) the amount of data transferred (*i.e.*, AW-EW traffic for *sequential replay* and *parallel replay*, and AW-checkpoint-store traffic for TARRAGON), and (3) the GPU recomputation cost (GPU-time) incurred by the alternate AW.

Fig. 12(a–c) summarizes the results. As the failure point increases, *sequential replay* has a steep increase in all three metrics: restoration time and GPU-time both grow roughly linearly with the increase of failure point, since the alternate AW must rerun attention for every layer and token, resulting in additional AW-EW traffic. *Parallel replay* still incurs the same amount of AW-EW traffic as *sequential replay*, growing rapidly with the failure point. *Parallel replay* incurs smaller restoration delays than *sequential replay*, but is still roughly an order of magnitude higher than TARRAGON (10 \times).

It is important to see that TARRAGON’s per-request restoration remains nearly constant and efficient across all tested failure points. GPU recomputation cost and total restoration

time are both negligible, as no prefill/decoding work is replayed. The amount of data transferred in TARRAGON is roughly 1/8 of that in *sequential replay* and *parallel replay*. Restoring the KV cache for a single request is far cheaper than regenerating it (up to 1800 \times latency reduction compared to *sequential replay*). As a result, AW-side self-healing under TARRAGON can recover from failures quickly and in an isolated manner, without flooding the network or burning scarce GPU cycles. This complements the end-to-end failover results in §7.2, showing that TARRAGON not only hides failures at the token-processing level but also bounds the system-wide recovery cost.

8 Related Work

Optimizations on MoE serving. Recent work on MoE serving has primarily focused on efficiency—reducing resource usage, improving GPU utilization, and lowering communication overhead [18, 25, 26, 36, 45]. These systems, however, retain static expert placement, fixed communication groups, and tightly synchronized AW-EW execution, causing a single worker failure to trigger coarse-grained restarts with no worker-level failover. TARRAGON complements these efficiency-oriented designs by introducing a reconfigurable datapath and bidirectional self-healing that confine and recover AW and EW failures at worker granularity.

Fault tolerance in LLM serving. Existing resilient serving approaches primarily target predictable events. For instance, SpotServe [29] adapts parallelism during preemption windows on cloud spot instances but does not handle sudden failures nor exploit the structure of decoupled attention-expert deployments. For KV cache durability and scalability, systems such as MoonCake [32] build a distributed KV cache store. TARRAGON is orthogonal to these efforts: it provides fine-grained failover for both AWs and EWs and can optionally integrate such a store to further strengthen KV cache recovery.

Fault tolerance in LLM training. Resilient training systems address failures through checkpointing [8], expert replica placement strategies [43], redundant computations [40], and state reconstruction from healthy replicas [19]. These techniques are effective for long-running, globally synchronized training jobs, but operate in a fundamentally different regime from inference, which must recover within tight latency budgets and preserve KV cache state.

9 Conclusion

Based on understanding the deficiencies of coarse-grained failover in today’s MoE serving frameworks, we developed TARRAGON. TARRAGON confines failure domains to individual workers, maintains forward progress of inference pipelines under failures, and limits the amount of processing required for recovery. Our evaluation shows that TARRAGON

cuts failure-induced stalls by up to 160–213× compared to state-of-the-art MoE serving frameworks, while matching their throughput when no failures occur. We believe these results demonstrate that strong failure resilience and high-performance MoE serving are not at odds, and that TARRAGON provides a practical solution for making large-scale LLM inference robust to the routine GPU and node failures seen in production clusters.

References

- [1] Multi-Process Service. <https://docs.nvidia.com/deploy/mps/index.html>, 2025. [ONLINE].
- [2] NCCL: Optimized primitives for collective multi-gpu communication <https://github.com/nvidia/nccl>, 2025.
- [3] ShareGPT. <https://sharegpt.com/>, 2025. [ONLINE].
- [4] The Llama 4 herd: The beginning of a new era of natively multimodal AI innovation. <https://ai.meta.com/blog/llama-4-multimodal-intelligence/>, 2025. [ONLINE].
- [5] Amey Agrawal, Nitin Kedia, Ashish Panwar, Jayashree Mohan, Nipun Kwatra, Bhargav Gulavani, Alexey Tumanov, and Ramachandran Ramjee. Taming Throughput-Latency tradeoff in LLM inference with Sarathi-Serve. In *18th USENIX Symposium on Operating Systems Design and Implementation (OSDI 24)*, pages 117–134, Santa Clara, CA, July 2024. USENIX Association.
- [6] Joshua Ainslie, James Lee-Thorp, Michiel de Jong, Yury Zemlyanskiy, Federico Lebrón, and Sumit Sanghai. Gqa: Training generalized multi-query transformer models from multi-head checkpoints, 2023.
- [7] Wei An, Xiao Bi, Guanting Chen, Shanhuang Chen, Chengqi Deng, Honghui Ding, Kai Dong, Qiushi Du, Wenjun Gao, Kang Guan, Jianzhong Guo, Yongqiang Guo, Zhe Fu, Ying He, Panpan Huang, Jiashi Li, Wenfeng Liang, Xiaodong Liu, Xin Liu, Yiyuan Liu, Yuxuan Liu, Shanghaio Lu, Xuan Lu, Xiaotao Nie, Tian Pei, Junjie Qiu, Hui Qu, Zehui Ren, Zhangli Sha, Xuecheng Su, Xiaowen Sun, Yixuan Tan, Minghui Tang, Shiyu Wang, Yaohui Wang, Yongji Wang, Ziwei Xie, Yiliang Xiong, Yanhong Xu, Shengfeng Ye, Shuiping Yu, Yukun Zha, Liyue Zhang, Haowei Zhang, Mingchuan Zhang, Wentao Zhang, Yichao Zhang, Chenggang Zhao, Yao Zhao, Shangyan Zhou, Shunfeng Zhou, and Yuheng Zou. Fire-flyer ai-hpc: A cost-effective software-hardware co-design for deep learning. In *Proceedings of the International Conference for High Performance Computing, Networking, Storage, and Analysis, SC ’24*. IEEE Press, 2024.
- [8] Sanjith Athlur, Nitika Saran, Muthian Sivathanu, Ramachandran Ramjee, and Nipun Kwatra. Varuna: scalable, low-cost training of massive deep learning models. In *Proceedings of the Seventeenth European Conference on Computer Systems, EuroSys ’22*, page 472–487, New York, NY, USA, 2022. Association for Computing Machinery.
- [9] Shengkun Cui, Archit Patke, Ziheng Chen, Aditya Ranjan, Hung Nguyen, Phuong Cao, Saurabh Jha, Brett Bode, Gregory Bauer, Chandra Narayanaswami, Daby Sow, Catello Di Martino, Zbigniew T. Kalbarczyk, and Ravishankar K. Iyer. Characterizing gpu resilience and impact on ai/hpc systems, 2025.
- [10] Damai Dai, Chengqi Deng, Chenggang Zhao, R. X. Xu, Huazuo Gao, Deli Chen, Jiashi Li, Wangding Zeng, Xingkai Yu, Y. Wu, Zhenda Xie, Y. K. Li, Panpan Huang, Fuli Luo, Chong Ruan, Zhifang Sui, and Wenfeng Liang. Deepseekmoe: Towards ultimate expert specialization in mixture-of-experts language models, 2024.
- [11] DeepSeek-AI. Deepseek-r1: Incentivizing reasoning capability in llms via reinforcement learning, 2025.
- [12] DeepSeek-AI. Deepseek-v3.2: Pushing the frontier of open large language models, 2025.
- [13] Aleksandar Dragojević, Dushyanth Narayanan, Miguel Castro, and Orion Hodson. FARM: Fast remote memory. In *11th USENIX Symposium on Networked Systems Design and Implementation (NSDI 14)*, pages 401–414, Seattle, WA, April 2014. USENIX Association.
- [14] William Fedus, Barret Zoph, and Noam Shazeer. Switch transformers: Scaling to trillion parameter models with simple and efficient sparsity. *Journal of Machine Learning Research*, 23(120):1–39, 2022.
- [15] Yao Fu, Leyang Xue, Yeqi Huang, Andrei-Octavian Brabete, Dmitrii Ustiugov, Yuvraj Patel, and Luo Mai. ServerlessLLM: Low-Latency serverless inference for large language models. In *18th USENIX Symposium on Operating Systems Design and Implementation (OSDI 24)*, pages 135–153, Santa Clara, CA, July 2024. USENIX Association.
- [16] Junhao Hu, Jiang Xu, Zhixia Liu, Yulong He, Yuetao Chen, Hao Xu, Jiang Liu, Jie Meng, Baoquan Zhang, Shining Wan, Gengyuan Dan, Zhiyu Dong, Zhihao Ren, Changhong Liu, Tao Xie, Dayun Lin, Qin Zhang, Yue Yu, Hao Feng, Xusheng Chen, and Yizhou Shan. Deepserve: Serverless large language model serving at scale, 2025.

- [17] Qinghao Hu, Zhisheng Ye, Zerui Wang, Guoteng Wang, Meng Zhang, Qiaoling Chen, Peng Sun, Dahua Lin, Xiaolin Wang, Yingwei Luo, Yonggang Wen, and Tianwei Zhang. Characterization of large language model development in the datacenter. In *21st USENIX Symposium on Networked Systems Design and Implementation (NSDI 24)*, pages 709–729, Santa Clara, CA, April 2024. USENIX Association.
- [18] Haiyang Huang, Newsha Ardalani, Anna Sun, Liu Ke, Hsien-Hsin S. Lee, Shruti Bhosale, Carole-Jean Wu, and Benjamin Lee. Toward efficient inference for mixture of experts. In A. Globerson, L. Mackey, D. Belgrave, A. Fan, U. Paquet, J. Tomczak, and C. Zhang, editors, *Advances in Neural Information Processing Systems*, volume 37, pages 84033–84059. Curran Associates, Inc., 2024.
- [19] Insu Jang, Zhenning Yang, Zhen Zhang, Xin Jin, and Mosharaf Chowdhury. Ooblec: Resilient distributed training of large models using pipeline templates. In *Proceedings of the 29th Symposium on Operating Systems Principles*, SOSP ’23, page 382–395, New York, NY, USA, 2023. Association for Computing Machinery.
- [20] Albert Q. Jiang, Alexandre Sablayrolles, Antoine Roux, Arthur Mensch, Blanche Savary, Chris Bamford, Devendra Singh Chaplot, Diego de las Casas, Emma Bou Hanna, Florian Bressand, Gianna Lengyel, Guillaume Bour, Guillaume Lample, Lélio Renard Lavaud, Lucile Saulnier, Marie-Anne Lachaux, Pierre Stock, Sandeep Subramanian, Sophia Yang, Szymon Antoniak, Teven Le Scao, Théophile Gervet, Thibaut Lavril, Thomas Wang, Timothée Lacroix, and William El Sayed. Mixtral of experts, 2024.
- [21] Ziheng Jiang, Haibin Lin, Yinmin Zhong, Qi Huang, Yangrui Chen, Zhi Zhang, Yanghua Peng, Xiang Li, Cong Xie, Shibiao Nong, Yulu Jia, Sun He, Hongmin Chen, Zhihao Bai, Qi Hou, Shipeng Yan, Ding Zhou, Yiyao Sheng, Zhuo Jiang, Haohan Xu, Haoran Wei, Zhang Zhang, Pengfei Nie, Leqi Zou, Sida Zhao, Liang Xiang, Zherui Liu, Zhe Li, Xiaoying Jia, Jianxi Ye, Xin Jin, and Xin Liu. MegaScale: Scaling large language model training to more than 10,000 GPUs. In *21st USENIX Symposium on Networked Systems Design and Implementation (NSDI 24)*, pages 745–760, Santa Clara, CA, April 2024. USENIX Association.
- [22] Anuj Kalia, Michael Kaminsky, and David G. Andersen. Using rdma efficiently for key-value services. *SIGCOMM Comput. Commun. Rev.*, 44(4):295–306, August 2014.
- [23] Woosuk Kwon, Zhuohan Li, Siyuan Zhuang, Ying Sheng, Lianmin Zheng, Cody Hao Yu, Joseph Gonzalez, Hao Zhang, and Ion Stoica. Efficient memory management for large language model serving with page-dattention. In *Proceedings of the 29th Symposium on Operating Systems Principles*, SOSP ’23, page 611–626, New York, NY, USA, 2023. Association for Computing Machinery.
- [24] Jiamin Li, Yimin Jiang, Yibo Zhu, Cong Wang, and Hong Xu. Accelerating distributed MoE training and inference with lina. In *2023 USENIX Annual Technical Conference (USENIX ATC 23)*, pages 945–959, Boston, MA, July 2023. USENIX Association.
- [25] Yan Li, Pengfei Zheng, Shuang Chen, Zewei Xu, Yuanhao Lai, Yunfei Du, and Zhengang Wang. Speculative moe: Communication efficient parallel moe inference with speculative token and expert pre-scheduling. *arXiv preprint arXiv:2503.04398*, 2025.
- [26] Aixin Liu, Bei Feng, Bing Xue, Bingxuan Wang, Bochao Wu, Chengda Lu, Chenggang Zhao, Chengqi Deng, Chenyu Zhang, Chong Ruan, et al. Deepseek-v3 technical report. *arXiv preprint arXiv:2412.19437*, 2024.
- [27] Ziming Liu, Boyu Tian, Guoteng Wang, Zhen Jiang, Peng Sun, Zhenhua Han, Tian Tang, Xiaohe Hu, Yanmin Jia, Yan Zhang, He Liu, Mingjun Zhang, Yiqi Zhang, Qiaoling Chen, Shenggan Cheng, Mingyu Gao, Yang You, and Siyuan Feng. Expert-as-a-service: Towards efficient, scalable, and robust large-scale moe serving, 2025.
- [28] Chiheng Lou, Sheng Qi, Chao Jin, Dapeng Nie, Haoran Yang, Yu Ding, Xuanzhe Liu, and Xin Jin. Hydraserve: Minimizing cold start latency for serverless llm serving in public clouds. In *21st USENIX Symposium on Networked Systems Design and Implementation (NSDI 24)*, 2026.
- [29] Xupeng Miao, Chunan Shi, Jiangfei Duan, Xiaoli Xi, Dahua Lin, Bin Cui, and Zhihao Jia. Spotserve: Serving generative large language models on preemptible instances. In *Proceedings of the 29th ACM International Conference on Architectural Support for Programming Languages and Operating Systems, Volume 2*, ASPLOS ’24, page 1112–1127, New York, NY, USA, 2024. Association for Computing Machinery.
- [30] OpenAI. gpt-oss-120b & gpt-oss-20b model card, 2025.
- [31] Jackson Petty, Sjoerd Steenkiste, Ishita Dasgupta, Fei Sha, Dan Garrette, and Tal Linzen. The impact of depth on compositional generalization in transformer language models. In Kevin Duh, Helena Gomez, and Steven Bethard, editors, *Proceedings of the 2024 Conference of the North American Chapter of the Association for Computational Linguistics: Human Language Technologies*

- (Volume 1: Long Papers), pages 7239–7252, Mexico City, Mexico, June 2024. Association for Computational Linguistics.
- [32] Ruoyu Qin, Zheming Li, Weiran He, Jialei Cui, Feng Ren, Mingxing Zhang, Yongwei Wu, Weimin Zheng, and Xinran Xu. Mooncake: Trading more storage for less computation — a KVCache-centric architecture for serving LLM chatbot. In *23rd USENIX Conference on File and Storage Technologies (FAST 25)*, pages 155–170, Santa Clara, CA, February 2025. USENIX Association.
- [33] Noam Shazeer. Fast transformer decoding: One write-head is all you need, 2019.
- [34] Noam Shazeer, Azalia Mirhoseini, Krzysztof Maziarz, Andy Davis, Quoc Le, Geoffrey Hinton, and Jeff Dean. Outrageously large neural networks: The sparsely-gated mixture-of-experts layer. *arXiv preprint arXiv:1701.06538*, 2017.
- [35] Chenchen Shou, Guyue Liu, Hao Nie, Huaiyu Meng, Yu Zhou, Yimin Jiang, Wenqing Lv, Yelong Xu, Yuanwei Lu, Zhang Chen, Yanbo Yu, Yichen Shen, Yibo Zhu, and Dixin Jiang. Infinitehbd: Building datacenter-scale high-bandwidth domain for llm with optical circuit switching transceivers, 2025.
- [36] StepFun. Step-3 is large yet affordable: Model-system co-design for cost-effective decoding, 2025.
- [37] Biao Sun, Ziming Huang, Hanyu Zhao, Wencong Xiao, Xinyi Zhang, Yong Li, and Wei Lin. Llumnix: Dynamic scheduling for large language model serving. In *18th USENIX Symposium on Operating Systems Design and Implementation (OSDI 24)*, pages 173–191, Santa Clara, CA, July 2024. USENIX Association.
- [38] Kimi Team. Kimi k2: Open agentic intelligence, 2025.
- [39] Qwen Team. Qwen3 technical report, 2025.
- [40] John Thorpe, Pengzhan Zhao, Jonathan Eyolfson, Yifan Qiao, Zhihao Jia, Minjia Zhang, Ravi Netravali, and Guoqing Harry Xu. Bamboo: Making preemptible instances resilient for affordable training of large DNNs. In *20th USENIX Symposium on Networked Systems Design and Implementation (NSDI 23)*, pages 497–513, Boston, MA, April 2023. USENIX Association.
- [41] Xingda Wei, Jiaxin Shi, Yanzhe Chen, Rong Chen, and Haibo Chen. Fast in-memory transaction processing using rdma and htm. In *Proceedings of the 25th Symposium on Operating Systems Principles, SOSP ’15*, page 87–104, New York, NY, USA, 2015. Association for Computing Machinery.
- [42] Yongji Wu, Xueshen Liu, Shuowei Jin, Ceyu Xu, Feng Qian, Z Morley Mao, Matthew Lentz, Danyang Zhuo, and Ion Stoica. Hetermoe: Efficient training of mixture-of-experts models on heterogeneous gpus. *arXiv preprint arXiv:2504.03871*, 2025.
- [43] Yongji Wu, Wenjie Qu, Tianyang Tao, Zhuang Wang, Wei Bai, Zhuohao Li, Yuan Tian, Jiaheng Zhang, Matthew Lentz, and Danyang Zhuo. Lazarus: Resilient and elastic training of mixture-of-experts models with adaptive expert placement. *arXiv preprint arXiv:2407.04656*, 2024.
- [44] Lianmin Zheng, Liangsheng Yin, Zhiqiang Xie, Chuyue Sun, Jeff Huang, Cody Hao Yu, Shiyi Cao, Christos Kozyrakis, Ion Stoica, Joseph E. Gonzalez, Clark Barrett, and Ying Sheng. Sqlang: Efficient execution of structured language model programs, 2024.
- [45] Ruidong Zhu, Ziheng Jiang, Chao Jin, Peng Wu, Cesar A. Stuardo, Dongyang Wang, Xinlei Zhang, Huaping Zhou, Haoran Wei, Yang Cheng, Jianzhe Xiao, Xinyi Zhang, Lingjun Liu, Haibin Lin, Li-Wen Chang, Jianxi Ye, Xiao Yu, Xuanzhe Liu, Xin Jin, and Xin Liu. Megascale-infer: Efficient mixture-of-experts model serving with disaggregated expert parallelism. In *Proceedings of the ACM SIGCOMM 2025 Conference, SIGCOMM ’25*, page 592–608, New York, NY, USA, 2025. Association for Computing Machinery.
- [46] Siyuan Zhuang, Zhuohan Li, Danyang Zhuo, Stephanie Wang, Eric Liang, Robert Nishihara, Philipp Moritz, and Ion Stoica. Hoplite: efficient and fault-tolerant collective communication for task-based distributed systems. In *Proceedings of the 2021 ACM SIGCOMM 2021 Conference, SIGCOMM ’21*, page 641–656, New York, NY, USA, 2021. Association for Computing Machinery.

A Failure Propagation in Monolithic and Decoupled Deployments

A.1 Case study I: monolithic deployment mode

Fig. 3 (a) presents how a single worker’s failure propagates in a monolithic deployment. When *Worker 1* fails during decoding, the collective communicator (CCL) is torn down after a timeout. Importantly, the CCL treats the set of workers as a static communication group [46]: if one worker becomes unavailable, the entire communicator aborts. Consequently, all workers are killed and restarted and the CCL is re-initialized. Then all workers must replay all L prefill layers, all decoding layers for the $(i-1)$ tokens that have already been produced, and finally the first ℓ layers for the current token have to be re-executed. All previously accumulated KV caches and partial outputs—even on healthy workers—are discarded. This results in a long, user-visible inference stall and substantial recomputation overhead.

A.2 Case study II: decoupled deployment mode

AW failure: Fig. 3 (b) shows the failure of a single AW. Upon failure, only the failed AW is restarted and reinitialized. Because the KV cache and frontier state for its requests are lost, the restarted AW must re-run the prefill and decode from the beginning (along with the corresponding EW computation) until it reaches the *same frontier* (layer ℓ of the i -th token) as the rest of the pipeline. Meanwhile, EWs must wait at the layer-wise synchronization barrier, stalling the entire inference pipeline until the failed AW catches up. Thus, despite preserving healthy workers, recovery still incurs long stalls and extensive recomputation, closely mirroring the monolithic case. The healthy workers remain running and merely wait at the synchronization barrier, without doing the recomputation.

EW failure: An EW failure behaves differently but still introduces an inference stall, as depicted in Fig. 3(c). Since EWs are stateless, an EW failure does not result in discarding previously computed KV caches or decoding progress preserved on the AWs. Thus, the failed EW needs to be restarted. Once the replacement EW is ready, it can recompute the expert output only at the current frontier ℓ . However, the AW that routed tokens to the failed EW must wait at the current *frontier* (layer ℓ) until the replacement EW is back online. As a result, decoding still experiences a user-visible stall, despite minimal recomputation.

B Expert Batch Size

Sparse expert activation also has a subtle but important side effect: it fragments tokens across many experts and leads to small per-expert batches. In our measurements on Qwen3-MoE, even when the *total* token batch size is 821, the vast

majority of per-expert batches contain fewer than 200 tokens (Fig. 13 (a)). However, on an NVIDIA A100, expert kernels only reach their throughput “knee point” at batch sizes of roughly 256~512 tokens (*i.e.*, an exponential growth of latency in Fig. 13 (b)), so most expert invocations run far below the GPU’s efficient operating regime. When attention layers and experts are co-located on the same GPUs, the memory-bound attention computation further constrains batch size, compounding underutilization (also observed in [45]).

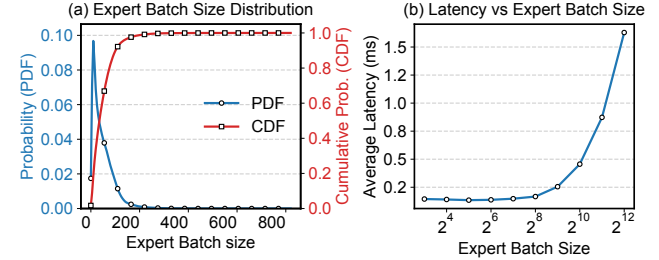


Figure 13: (a) Run total batch size of 821 and collect the expert batch size distribution of Qwen3-MoE [39] across different layers. (b) The single expert computation latency of Qwen3-MoE [39] on 8 x Nvidia A100 with different expert batch sizes.

C Checkpointing Overhead Analysis

Checkpoint overhead is dominated by the size of each incremental KV cache segment, which is:

$$C = 2 \times H_{\text{kv}} \times \frac{N_{\text{hidden_size}}}{H_{\text{attn}}} \times S_{\text{elem}}$$

where $N_{\text{hidden_size}}$ is the hidden size and S_{elem} is the number of bytes per tensor element. H_{kv} and H_{attn} are the numbers of KV heads and attention heads, respectively.

In memory-efficient attention mechanisms such as multi-query attention (MQA) and grouped-query attention (GQA) [6, 33], $H_{\text{kv}} \ll H_{\text{attn}}$, substantially reducing checkpointing traffic. By contrast, the per-token, per-layer communication volume between the AW and EW is:

$$V = 2 \times \text{Top}_k \times N_{\text{hidden_size}} \times S_{\text{elem}}$$

which is significantly larger (Top_k is the number of expert chosen per layer). For example, in Mixtral-8x7B [20], incremental KV cache traffic is only $\sim 12.5\%$ of expert traffic.

D Inactive Shadow Experts During Normal Execution

We find that executing two experts concurrently (Concurrent Exec) with two CUDA streams results in significant interference compared with activating only a single expert (Single

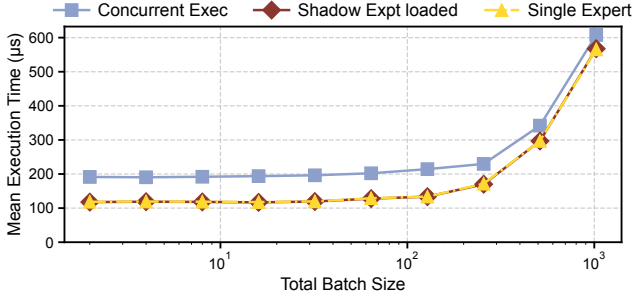


Figure 14: Impact of shadow expert on execution latency

Expert), using the same total batch size. As shown in Fig. 14, the computation latency of activating a single expert (Single Expert) is identical to the latency of loading an additional shadow expert, but not activating it (Shadow Expt Loaded). Without failures, the loaded shadow expert consumes GPU memory but does not introduce any computational overhead for the activated expert.

E Implementation of Lightweight Failure Detection

We implement the explicit probes as “zero-length” RDMA writes, a no-op operation that incurs minimal overhead. To track the status of probes, each worker monitors its RDMA Completion Queue (CQ) to inspect the `ibv_wc_status` of the relevant QP (data-plane QP for the implicit probe and control-plane QP for the explicit probe). If a probe experiences a small number of consecutive timeouts (default value is 3, configured at QP initialization in TARRAGON), the RNIC marks the QP with `IBV_WC_RETRY_EXC_ERR` (raises `IBV_WC_WR_FLUSH_ERR` for work requests in CQ), and flushes all pending work requests on that QP. TARRAGON interprets these hardware-level signals as a fail-stop event on the corresponding peer (either a worker or link failure) and immediately hands them to the recovery logic to trigger self-healing and worker replacement.

F Ablation Study

We perform an ablation study on TARRAGON’s main resiliency components to understand their individual contribution to overall performance, including: (i) incremental KV cache checkpointing (§6.1) (ii) lightweight failure detection; (iii) the ERT used for dynamic expert remapping (§4.2).

We evaluate three variants of TARRAGON: (Alt-1) disables KV cache checkpointing/restoration; (Alt-2) additionally disables failure detection; (Alt-3) further disables the ERT. We use the same model and workloads as in §7.3 and vary the request arrival rate. In this experiment, we *do not inject failures* so that any performance differences are purely due to the steady-state overheads of these components. We report end-to-end inference throughput in terms of output tokens/sec.

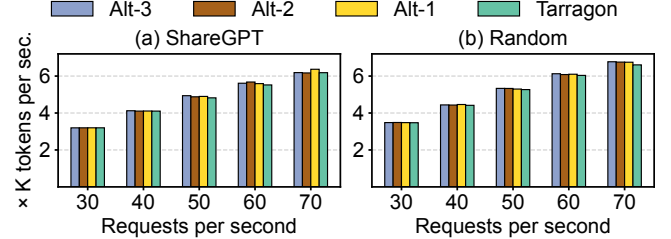


Figure 15: Ablation study of TARRAGON’s main resilience components. We evaluate output tokens per second for (a) ShareGPT and (b) Random.

Fig. 15 shows that across all request rates and workloads, the throughput of all alternatives is nearly indistinguishable: the maximum deviation stays within 3%. In particular, TARRAGON with all components enabled matches the no-resiliency baseline (Alt-3, similar to MegaScale-Infer), for this no-failure case.